Pattern Recognition 42 (2009) 1172 – 1179

Contents lists available at ScienceDirect

Pattern Recognition

journal homepage: www.elsevier.com/locate/pr

A multi-direction GVF snake for the segmentation of skin cancer images

Jinshan Tang*

Image Processing and Bio-imaging Research Laboratory, Systems Research Institute and Department of Advanced Technologies, Alcorn State University, Lorman, MS 39096, USA

ARTICLE INFO

Article history:
Received 28 March 2008
Received in revised form 4 September 2008
Accepted 16 September 2008

Keywords:
Skin tumor
Boundary extraction
Gradient vector flow
Active contour
Multidirection

ABSTRACT

A multi-direction gradient vector flow (GVF) snake-based scheme is proposed in this paper for the segmentation of skin cancer images. Unlike the traditional anisotropic diffusion (AD) filter, which has many disadvantages such as sensitivity to noise, a new AD filter has been developed to remove the noise. The proposed AD filter uses adaptive threshold selection and a new gradient computation method, which is robust to noise and can effectively remove the hairs. After the noise is removed from the skin cancer image, the image is segmented using a multi-direction GVF snake. The multi-direction GVF snake extends the single direction GVF snake and traces the boundary of the skin cancer even if there are other objects near the skin cancer region. Experiments performed on 11 cancer images show the effectiveness of the proposed algorithm.

1. Introduction

The incidence of skin cancer is rapidly increasing throughout the world [1]. In order to reduce the morbidity of skin cancer, computer-aided detection and diagnosis technologies have been developed. The extraction of the skin cancer border is a key technology in computer-aided detection technologies for skin cancer diagnosis.

In the past, several skin cancer border extraction technologies have been proposed. In Ref. [2], a radial search technique is proposed to detect the border of the tumor. In this method, the RGB image is converted to a gray intensity image and two radial search techniques are then used to find the border of the skin cancer. The first radial search is an independent search, which is used to find the seed border points. The second radial search is used to track the border based on the nearest border point. In Ref. [3], a color-based segmentation algorithm is proposed. The algorithm is composed of several steps. The first step is to use a pseudomedian filter to remove the noise and then use color to segment the image into different objects with varying sizes. After that, a morphological opening-closing operator is adopted to reduce the data. Finally, the object determined to be most likely the tumor object is labeled as *candidate tumor object*. The contour is located using a contour encoding algorithm called Freeman Chain Coding. Another color-based skin tumor boundary detection method is presented in Ref. [4]. In this method, the RGB color space is converted to another color space and color segmentation is performed in the new color space. After the image is segmented, the tumor image and the border are extracted from the segmented image. In Ref. [5], an automatic method for image segmentation is developed. This method includes preprocessing, initial segmentation, and region refinement stages. In the preprocessing stage, a color image is transformed into an intensity image which suppresses the variations in the tumor region. The second stage is initial segmentation. In this stage, the gray thresholding method is employed to find the approximate boundaries of the lesion. The region refinement stage refines the segmentation result in the second stage. This involves initializing a closed elastic curve at the approximate boundary and then shrinking and expanding it to fit the edges in its neighborhood [5]. In Ref. [6], a skin tumor segmentation method based on partial differential equation (PDE) is presented. This method includes contrast enhancement and noise reduction in its preprocessing stage. This removes the noise and enhances the contrast of the tumor images. The segmentation algorithm is a geodesic active contour model. This method is especially effective when the skin lesion is covered with a large amount of hair. Because different segmentation methods have their advantages and disadvantages, a segmentation method fusing different methods is proposed in Ref. [7]. This method fuses global thresholding, dynamic thresholding, and 3-D color clustering and provides better results than individual methods.

In this paper, we will investigate skin cancer segmentation using an active contour model, or snake model, driven by a GVF. A snake is a parameterized contour [8] that translates and deforms on the image plane according to the strength of the image's edges and the internal properties of the contour such as smoothness. Since the introduction of the original snake by Kass et al. [8], many other snakes

* Tel.: +1 601 877 2479; fax: +1 601 877 3941.
E-mail address: jtang@alcorn.edu

0031-3203/$ - see front matter © 2008 Elsevier Ltd. All rights reserved.
doi:10.1016/j.patcog.2008.09.007

have been proposed [9,10]. This paper adopts a gradient vector flow (GVF) snake originally developed and discussed in Ref. [9]. The advantage of a GVF snake is its robustness to the initialization of the snake [9–11]. Although a GVF snake is robust to the initialization of the snake, it is still sensitive to image noise [12]. In order to make the snake insensitive to noise and be able to remove the hairs, an AD filter is proposed. After the noise and hairs are removed, a multi-direction GVF snake will be used to segment the skin cancer region. The multi-direction GVF snake extends the single direction GVF snake and allows it to still be able to track the boundary of the skin cancer even if there are other objects near the skin cancer region.

2. Preprocessing using AD

2.1. Anisotropic diffusion

AD has been applied to reduce the noise in images and has produced good results in past trials [13–17]. AD is a nonlinear filtering method, which encourages diffusion in the homogeneous region while inhibiting diffusion at the edges. The PDE of AD is given as follows in a continuous domain [13,14,16]

$$\begin{cases} \dfrac{\partial I}{\partial t} = \mathrm{div}[c(|\nabla I|)\nabla I] \\ I(t=0) = I_0 \end{cases} \tag{1}$$

where ∇ is the gradient operator, *div* is the divergence operator, $||$ denotes the magnitude, I_0 is the initial image and $c()$ is the diffusion coefficient. $c()$ is often chosen such that $c(x)\to 0$ as $x\to\infty$ and should be monotonically decreasing. The diffusion decreases as the gradient strength increases, and the diffusion stops across edges. Several $c()$ have been suggested for the diffusion [13,14,16]:

$$c(x) = \exp\left(-\left[\frac{x}{k}\right]^2\right) \tag{2}$$

$$c(x) = \frac{1}{1+[x^2-k^2]/[k^2(1+k^2)]} \tag{3}$$

where k is a parameter to control the diffusion extension.

A discrete form of Eq. (1) is given by [13,14,16]:

$$I_s^{t+\Delta t} = I_s^t + \frac{\Delta t}{|\overline{\eta}_s|}\sum_{p\in\overline{\eta}_s} c(\nabla I_{s,p}^t)\nabla I_{s,p}^t \tag{4}$$

where $I_s{}^t$ is the discretely sampled image, s denotes the pixel position in a discrete 2-D grid, and Δt is the time step size, $\overline{\eta}_s$ represents the spatial neighborhood of pixel s, $|\overline{\eta}_s|$ is the number of pixels in the window, and $\nabla I_{s,p}{}^t = I_p{}^t - I_s{}^t$, $\forall p \in \overline{\eta}_s$.

In AD, the representation of edges and the choice of k in the diffusion coefficient are very important. The ideal choice of edge representation method and k in the diffusion coefficient will achieve an efficient AD algorithm.

2.2. An adaptive AD

As described in Section 2.1, the representation of the edge is very important to achieve an efficient AD filter. The gradient magnitude operator, as proposed by Eq. (1), is sensitive to noise, especially when the strength of the edge is weak. In order to alleviate this situation, we use the following gradient magnitude as the representation of the edge [16],

$$f(i,j) = \sqrt{\frac{|\nabla I_W(i,j)|^2 + |\nabla I_E(i,j)|^2 + |\nabla I_S(i,j)|^2 + |\nabla I_N(i,j)|^2}{4}} \tag{5}$$

$$\nabla I_E(i,j) = I(i,j+1) - I(i,j) \tag{6}$$

$$\nabla I_W(i,j) = I(i,j-1) - I(i,j) \tag{7}$$

$$\nabla I_S(i,j) = I(i+1,j) - I(i,j) \tag{8}$$

$$\nabla I_N(i,j) = I(i-1,j) - I(i,j) \tag{9}$$

By inserting Eq. (5) into Eq. (2) or (3), we can obtain the new computation of the diffusion coefficients as follows:

$$c(f) = \exp\left(-\left[\frac{f(x,y)}{k}\right]^2\right) \tag{10}$$

$$c(f) = \frac{1}{1+[f(x,y)^2 - k^2]/[k^2(1+k^2)]} \tag{11}$$

The computation of the diffusion coefficients adopts the gradient magnitude in Eq. (5) and has several advantages over the original. Because we use the average of the four direction gradients instead of the average of the two directional gradients, the new computation of the diffusion coefficients is more robust to noise than the original computation.

Let us consider the noise distribution in the image. Suppose we have a homogeneous region with noise only. We can assume that $\nabla I_E(i,j)$, $\nabla I_W(i,j)$, $\nabla I_S(i,j)$, $\nabla I_N(i,j)$ have the same zero mean normal distribution $N(0,\sigma^2)$. Thus,

$$\frac{4}{\sigma^2}f(i,j)^2 = \frac{1}{\sigma^2}(|\nabla I_W(i,j)|^2 + |\nabla I_E(i,j)|^2 + |\nabla I_S(i,j)|^2 + |\nabla I_N(i,j)|^2) \tag{12}$$

has a chi-squared distribution with four degrees of freedom.

After we get the distribution of the noise gradient, let us consider the computation of k in Eq. (2) or (3). Assume that i, j are the coordinates of a pixel in the image. We can use Eq. (5) to obtain its gradient map. After that, let us think how to select k so that the performance of the AD filter is improved. As is well known, in the original AD, k is a fixed value in each iteration which limits the performance of the AD filter. In order to improve the performance of the AD filter, we adopt the adaptive computation of k in each iteration.

From Ref. [18], we know that the edge points generally have large gradient values which are statistically outliers with respect to the chi-squared distribution described in Eq. (12). Thus we can use statistical test(chi-squared test) to test whether one pixel is edge point or not. If the pixel at (i,j) is an edge point, then $((4/\sigma^2)f(i,j)^2)$ will not follow chi-squared distribution described in Eq. (12). Based on chi-squared test theory, we need to find a threshold T (critical value) to determine whether a pixel is an edge point or not (if $((4/\sigma^2)f(i,j)^2) > T$, then the pixel is treated as an edge point). The threshold T can be obtained by minimizing the probability of type II error, which can be expressed as follows:

$$P\left(\frac{4}{\sigma^2} * f(i,j)^2 > T\right) = \alpha \tag{13}$$

where σ^2 is the variance of the noise gradient and T is the critical value which is determined by the value of α and can be obtained by looking-up the chi-squared test table. Now let us consider how to compute k in Eqs. (10) and (11). From Eqs. (10) and (11), k can be selected so that if $f(i,j)^2 > k^2$, then the pixel is treated as edge point. Combining with the statement that if $((4/\sigma^2)f(i,j)^2) > T$, then the pixel is treated as edge point, k can be selected as follows:

$$k^2 = \frac{\sigma^2}{4}T \tag{14}$$

Let $c = \sqrt{T}/2$, then k can be set as follows:

$$k = c\sigma \tag{15}$$

The key of the algorithm lies in the choice of the homogenous region that is used to estimate σ^2. Although the selection can be done

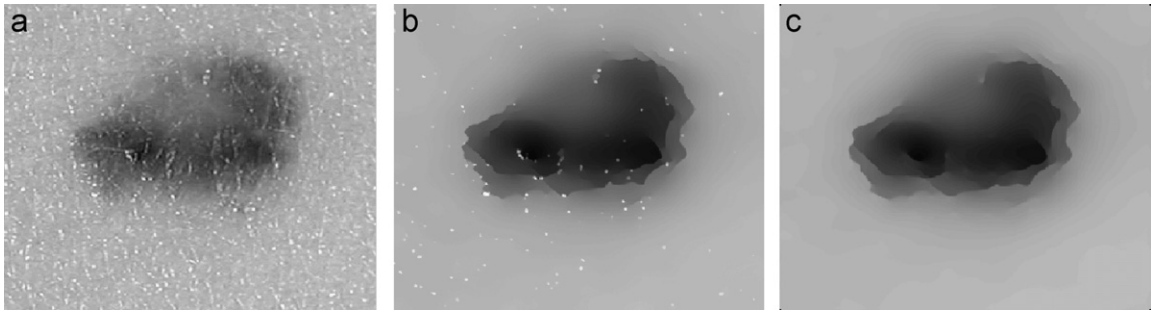

Fig. 1. The AD filter can remove the independent spots effectively: (a) original image; (b) filtered by anisotropic diffusion without median filter; (c) filtered by anisotropic diffusion with median filter.

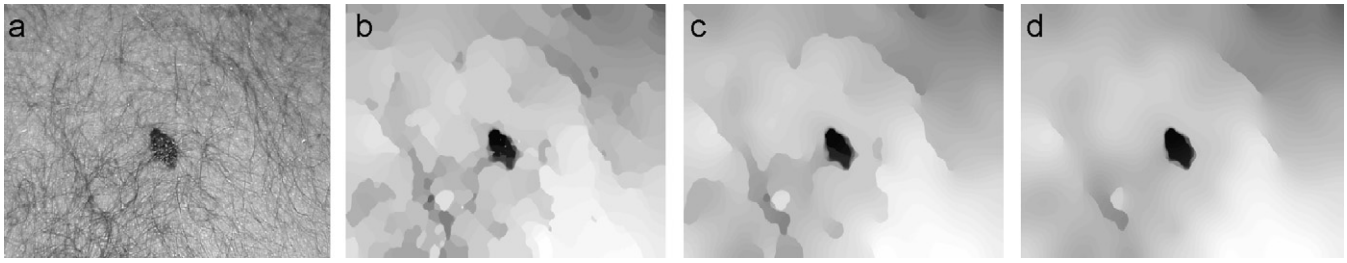

Fig. 2. Comparison of diffusion results with different significant levels: (a) original image; (b) $\alpha = 0.5$; (c) $\alpha = 0.05$; (d) $\alpha = 0.005$.

manually, it becomes more difficult if a large number of images need to be processed. Thus, we provide an automatic selection method. In this method, the image is first divided into several n by n small blocks. A contrast measure is then used to compute the homogeneity of each region. The contrast measure for a region is defined as

$$C = \frac{\sum_{(i,j)\in\Omega} C(i,j)}{N} \tag{16}$$

where Ω is an image region, N is the number of pixels in the region, and $C(i,j)$ is the contrast of the pixel (i,j), which is defined as

$$C(i,j) = \frac{I_{\max}(i,j) - I_{\min}(i,j)}{I_{\max}(i,j) + I_{\min}(i,j)} \tag{17}$$

where $I_{\max}(i,j)$ and $I_{\min}(i,j)$ are the maximum and minimum values in the neighborhood of the pixel (i,j). In this paper, the size of the neighborhood is 16×16.

After the contrast of each block is computed, they are sorted in order and only a fraction of the blocks are retained. In this paper, the three blocks (denoted by B_1, B_2, B_3) with the highest ranks are retained. Although more blocks can be used, our experiments found that three blocks is the best choice. The variance is estimated from these three blocks. The estimation of the variance σ^2 is composed of three steps: (1) In the first step, we compute the gradient of the three blocks (B_1, B_2, B_3) at each pixel using the equation $\nabla B_k(i,j) = B_k(i,j+1) - B_k(i,j)$, where $k = 1,2,3$. (2) In the second step, we use the obtained three blocks $\nabla B_k(i,j)$ $(k = 1,2,3)$ to reconstruct a larger block with the size of 16×48. If we denote the reconstructed block by ∇B, then the larger block reconstructed from $\nabla B_k(i,j)$ $(k = 1,2,3)$ is $\nabla B = [\nabla B_1 \ \nabla B_2 \ \nabla B_3]$. (3) In the third step, we use the variance of the gradient ∇B obtained at the second step as the value of σ^2. The benefit in the estimation of variance by concatenating three blocks instead of a whole block is to reduce the homogeneity requirements and to enhance the robustness of the estimation.

The new algorithm is adaptive and is image dependent for each iteration in the diffusion processing. Because there are independent spots in the image, we use the median filter to filter the image after AD. Fig. 1 shows the filtered image with and without the median filter after AD. It shows that with the median filter, we can remove the independent spots and hairs effectively.

In the proposed algorithm, the choice of the significant level α is very important. In the general statistics problems, the significant level is generally set to be 0.05. In our experiments, several values of significant level α were tested to get the suitable T. They are 0.0005, 0.005, 0.05, 0.25, 0.5 and 0.75. Our experiments show that 0.005 can produce the best results and thus T is set to be 14.8602 in this paper. Fig. 2 shows the different diffusion results obtained using different α's.

3. Segmentation of skin cancer images using multi-direction GVF snake

3.1. GGVF snake

Kass et al. [8] defined a snake as a controlled continuity contour that is attracted to salient image features and whose motion is enacted by minimizing the following energy functional:

$$E_{snake} = \int_0^1 [E_{\text{int}}(\mathbf{r}(s)) + E_{ext}(\mathbf{r}(s))]\,\mathrm{d}s \tag{18}$$

where the position of a snake can be represented parametrically by $\mathbf{r}(s) = (x(s),y(s))$, E_{int} and E_{ext} represent the internal energy and the external energy, respectively. The internal energy keeps the active contour smooth and may be defined as [8]

$$E_{\text{int}} = (\alpha|\mathbf{r}_s(s)|^2 + \beta|\mathbf{r}_{ss}(s)|^2)/2 \tag{19}$$

The external energy is application-based and is generally defined as

$$E_{ext}(\mathbf{r}(s)) = -|\nabla G_\sigma(x,y) * I(x,y)| \tag{20}$$

where $I(x,y)$ is the image intensity at (x,y), $G_\sigma(x,y)$ is a 2-D Gaussian kernel with the standard deviation σ, and ∇ is the gradient operator.

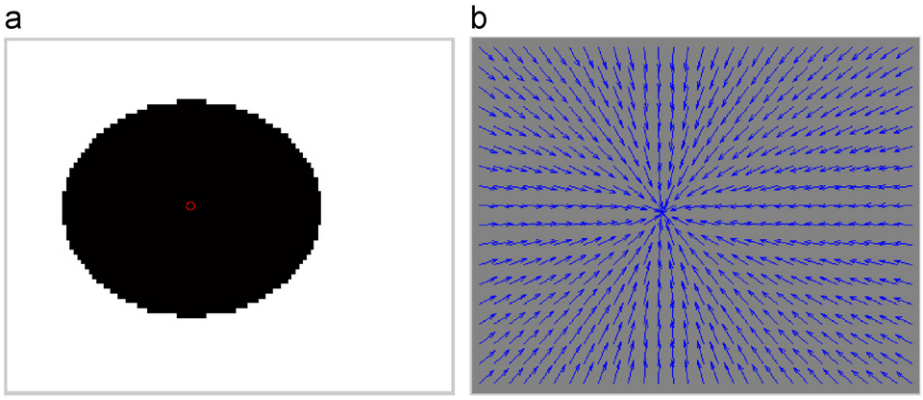

Fig. 3. Direction vector field: (a) a dark object and its center; (b) direction vector field.

By solving the minimization problem in Eq. (18) using variational calculus techniques, we can get a force balance equation [8]

$$\alpha x_{ss} - \beta x_{ssss} - \frac{\partial E_{ext}}{\partial x} = 0 \tag{21}$$

$$\alpha y_{ss} - \beta y_{ssss} - \frac{\partial E_{ext}}{\partial y} = 0 \tag{22}$$

where $(-\partial E_{ext}/\partial x, -\partial E_{ext}/\partial y)$ are the external forces. One of the disadvantages of using external forces $(-\partial E_{ext}/\partial x, -\partial E_{ext}/\partial y)$ is their sensitivity to the initialization of the snake. The initial contour must be close to the actual object boundary because the capture range of the image gradient is small. To alleviate this problem, GVF is proposed in Refs. [9,10] to replace the external force in Eqs. (21) and (22). A GVF (u, v) can be obtained by descending on the following energy function [9,10]:

$$E_{GGVF}(u,v) = \frac{1}{2}\int\int g(|\nabla f|)(u_x^2 + u_y^2 + v_x^2 + v_y^2) + (1 - g(|\nabla f|))((u - f_x)^2 + (v - f_y)^2)\,dx\,dy \tag{23}$$

where f is an edge map derived from the image and g is a decreasing function of the edge-force magnitude and is defined as follows:

$$g(|\nabla f|) = \exp\left(-\left(\frac{|\nabla f|}{K}\right)\right) \tag{24}$$

Here, K is a non-negative smoothing parameter for the field (u,v). The function described by Eq. (23) smoothes the force field (u,v) only when the edge strength is low. From Eq. (23), the following Euler equations can be obtained [9,10]:

$$g\nabla^2 u - (1 - g)(u - f_x) = 0 \tag{25}$$

$$g\nabla^2 v - (1 - g)(v - f_y) = 0 \tag{26}$$

The GVF field can be obtained by solving the following PDEs [9,10]:

$$u_t = g\nabla^2 u - (1 - g)(u - f_x) \tag{27}$$

$$v_t = g\nabla^2 v - (1 - g)(v - f_y) \tag{28}$$

By solving Eqs. (27) and (28), we can obtain the generalized GVF vectors, which can be used as external forces that attract the snake to the object boundary [9,10].

3.2. Multi-direction GGVF snake

In Ref. [11], a directional gradient vector flow (DGVF) snake model was developed. In this snake model, a fixed direction was used to compute the directional gradient and the directional gradient was then used to compute the DGVF. In this paper, we will extend the fixed DGVF flow to a multi-direction gradient vector flow. The basic idea is to compute the directional gradient for each pixel with a varying direction.

Suppose the center of an object is (c_1,c_2), which is defined as

$$c_1 = \frac{1}{N}\sum_{i=1}^{N} x_i, \quad c_2 = \frac{1}{N}\sum_{i=1}^{N} y_i$$

where (x_i,y_i) $(i = 1,2,\ldots,N)$ are the coordinates of the pixels in the object and N is the number of pixels in the object. Let $I(x,y)$ be the pixel value at location (x,y). The direction vector $\vec{d}(x,y)=(d_x,d_y)$ from (x,y) pointing to the center (c_1,c_2) of the object can be obtained using the following equations:

$$d_x = \frac{c_1 - x}{\sqrt{(c_1 - x)^2 + (c_2 - y)^2}} \tag{29}$$

$$d_y = \frac{c_2 - y}{\sqrt{(c_1 - x)^2 + (c_2 - y)^2}} \tag{30}$$

For each pixel in the image, we can obtain a direction vector. Thus, for the entire image we get a direction vector field. Fig. 3(b) shows the direction vector field of Fig. 3(a). Here we assume that the object in the synthetic image is known and the center of the object is marked manually before the direction vector field is computed.

After we obtain the direction vector field of an image, we can use it to compute the gradient along the direction $(\vec{d}(x,y) = (d_x,d_y))$ from each pixel pointing to the center of the object. The gradient for each pixel is computed in two steps. The first step is to find the approximate value of the direction vector $\vec{d}(x,y) = (d_x,d_y)$ from the vector set $V = \{\vec{v}|(v_x,v_y)\}$, where $v_x = -1$ or 0 or 1, $v_y = -1$ or 0 or 1, by minimizing the following distance measure:

$$dis(\vec{d},\vec{v}) = 1 - \frac{v_x d_x + v_y d_y}{\sqrt{v_x^2 + v_y^2}\sqrt{d_x^2 + d_y^2}} \tag{31}$$

Here $V = \{\vec{v}|(v_x,v_y)\}$ is a vector set composed of nine vectors: $(-1,-1)$, $(-1,0)$, $(-1,1)$, $(0,-1)$, $(0,0)$, $(0,1)$, $(1,-1)$, $(1,0)$, and $(1,1)$. The minimization of Eq. (31) is to select a vector from the nine vectors in set V such that the selected vector is closed to the direction vector $(\vec{d}(x,y) = (d_x,d_y))$. The second term in Eq. (31) is cosine similarity measurement which is used to measure the similarity of two directions. If the cosine similarity (ranging from 0 to 1) is high, then the similarity of two directions is high. The reason why we

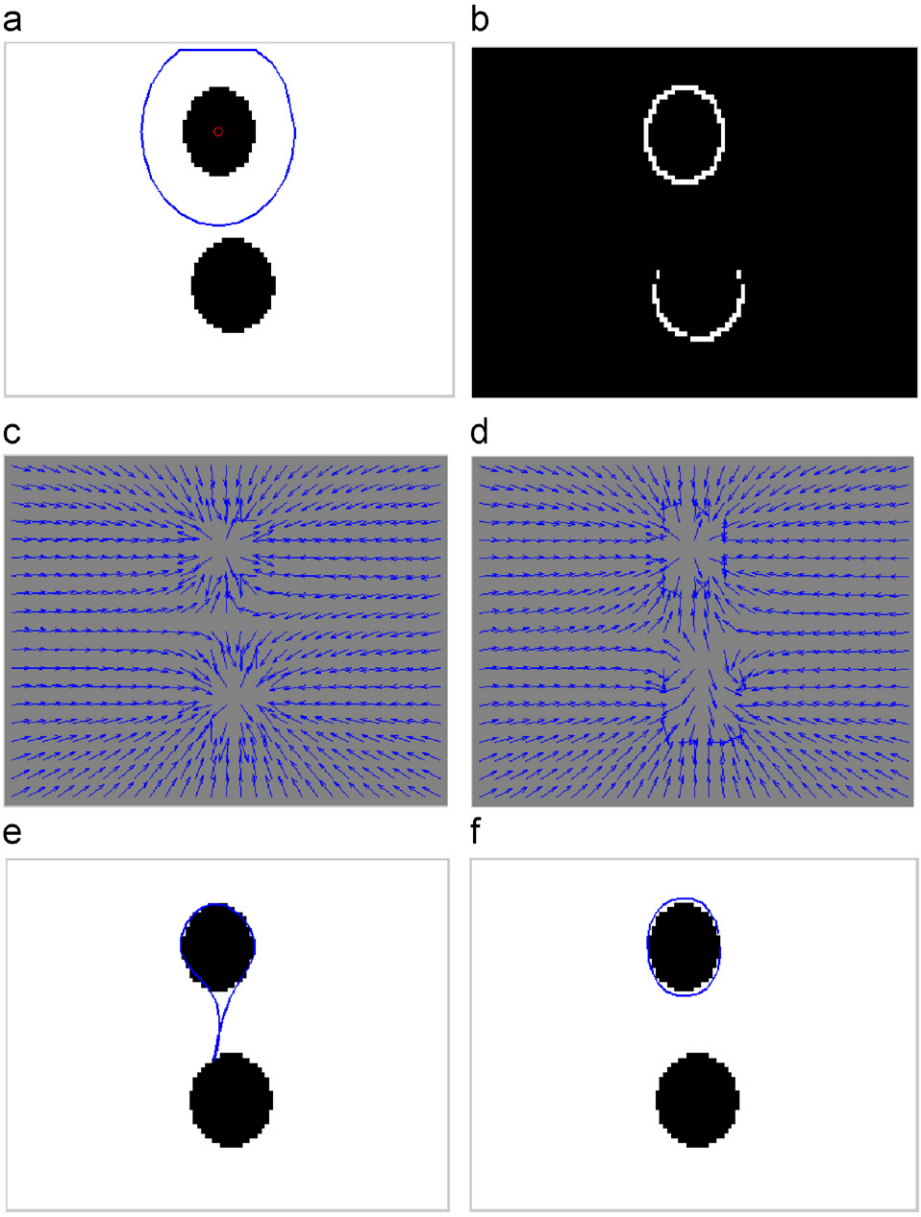

Fig. 4. Gradient vector flow and directional gradient vector flow: (a) boundary tracking using GVF snake: (a) two dark objects with a center on the above object and initialization of the snake; (b) directional gradient; (c) gradient vector flow; (d) directional gradient vector flow; (e) boundary tracking using GVF snake; (f) boundary tracking using directional GVF snake.

use the approximate values to replace the original direction vectors is to make the computation of the directional gradient in Eq. (32) simple. After the approximate values are used, only nine direction vectors are used when the directional gradient is computed and thus the computation is simplified. Denoting the approximate value of the direction vector at pixel $I(x,y)$ by $\hat{v}=(\hat{v}_x,\hat{v}_y)$, the directional gradient $DI(x,y)$ at pixel $I(x,y)$ can be computed as

$$DI(x,y)=I(x+\hat{v}_x,y+\hat{v}_y)-I(x,y) \tag{32}$$

Except for the lesion region, there are also other objects, such as rules, in the image. In some cases, there are more than one lesion region. In order to avoid the snake to converge to the wrong object, we rely on one fact in the skin cancer image: the lesion region is generally dark. Thus, we can avoid snake convergence of the wrong object, such as rules, by using the negative value of the directional gradient obtained in Eq. (32), which is expressed as

$$F(x,y)=\begin{cases} DI(x,y), & DI(x,y)<0 \\ 0 & \text{otherwise} \end{cases} \tag{33}$$

By replacing f with F in Eq. (23), we obtain the DGVF of the image by minimizing the following equation:

$$E_{\mathrm{GGVF}}(u,v)=\frac{1}{2}\int\int g(|\nabla F|)(u_x^2+u_y^2+v_x^2+v_y^2) + (1-g(|\nabla F|))((u-F_x)^2+(v-F_y)^2)\,\mathrm{d}x\,\mathrm{d}y \tag{34}$$

By solving Eq. (34), we can obtain equations similar to Eqs. (27) and (28). Fig. 4 shows the GVF and directional GVF when there are two dark objects in an image. From (c) and (d), we find that the flow is biased to the object in which the center is set on the object. For object boundary tracking, if the initial snake is close to the other

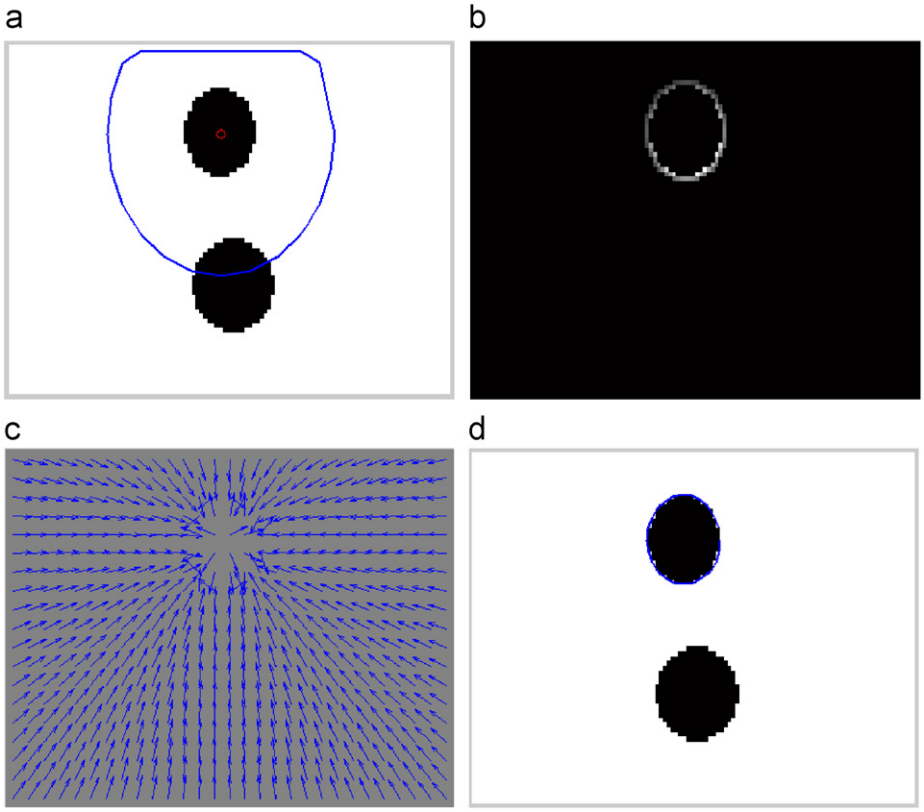

Fig. 5. Directional gradient flow with weighting gradient $F(x,y)$; $\beta = 0.8$: (a) initialization of the boundary of the snake; (b) weighting directional gradient; (c) directional GVF with the weighting gradient; (d) the final contour.

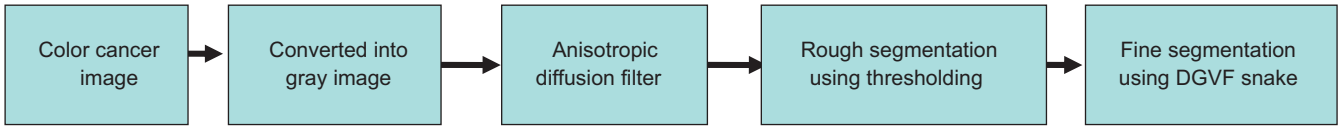

Fig. 6. General frame for skin cancer image segmentation.

object, the snake will not converge to the object we want to track if GVF is used (in this paper, we hope to extract the boundary of the upper object). However, if we use DGVF, the snake will converge to the real boundary of the object we want to track.

In order to weaken the affection of nearby objects when one object's boundary is extracted, we use weighting gradient, which is defined as follows:

$$F(x,y) = \begin{cases} DI(x,y)e^{\beta\sqrt{(c_1-x)^2+(c_2-y)^2}}, & DI(x,y) < 0 \\ 0 & \text{otherwise} \end{cases} \quad (35)$$

where β is a number which can be determined by the experiments. Fig. 5 shows the directional gradient flow with the weighting gradient and boundary extraction for the image in Fig. 4(a).

3.3. Segmentation of skin cancer images

The segmentation of skin cancer is described in Fig. 6. In the proposed algorithm, the color image is first converted into gray image. After that, the AD filter proposed in Section 2 is used to remove the noise and hairs. The filtered image is then performed by rough segmentation using a thresholding method developed in Ref. [19]. The rough contour of the cancer region is extracted. After rough segmentation, we use the rough segmentation results to obtain the center of the objects. The directional snake presented in Section 3.2 is used to obtain the final contour. Before the DGVF snake is employed to locate the final contour, the rough contour obtained using the thresholding method is enlarged 5 pixels larger than the original one and is used as the initial contour of the DGVF snake.

4. Experiments

In order to compare the segmentation performance of the proposed algorithm, we need a metric. The metric used in this paper is Pratt's quality measurement [20]. Pratt's quality measurement has been used for applications, especially for segmentation problems. Pratt's quality measurement metric (*FOM*) is defined as [20]

$$FOM = \frac{\sum_{i=1}^{I_A} \frac{1}{1+\alpha(d(i)^2)}}{\max(I_A, I_I)}$$

where I_A is the number of boundary pixels delineated by a computer-aided segmentation method, I_I is the number of boundary pixels delineated by the technicians, $d(i)$ is the Euclidean distance between a boundary pixel delineated by the technicians and the nearest boundary pixel delineated by computer-aided segmentation, and α is

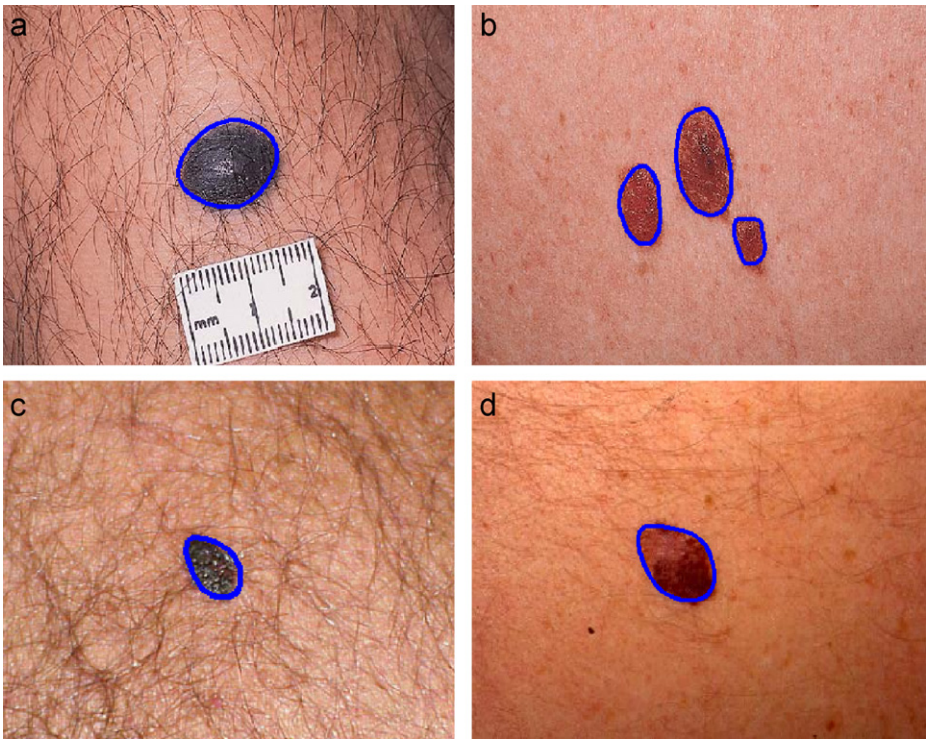

Fig. 7. Samples of skin cancer segmentation using the proposed algorithm: (a) lesion extraction with heavy hairs and a rule; (b) multi-lesion extraction; (c) lesion extraction with heavy hairs; (d) lesion extraction with varying light conditions in the background.

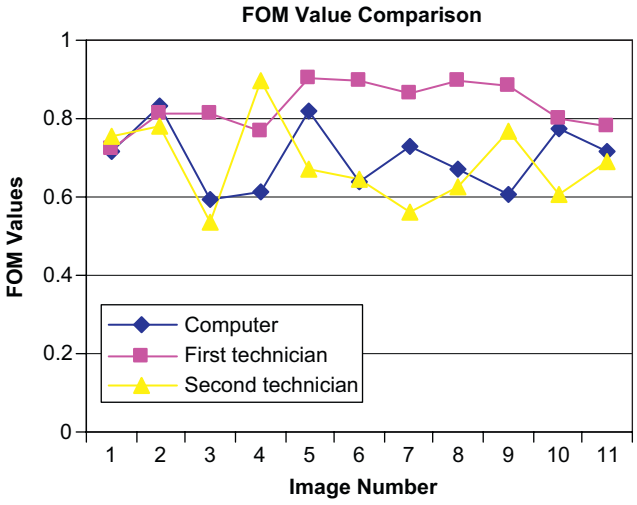

Fig. 8. Pratt's quality measurement for the computer based segmentation.

a scaling constant with a value of 0.05 in our experiments. The complete matching between the boundary pixels delineated by the computer-aided segmentation method and the boundary pixels delineated by the technicians has $FOM = 1$ in the equation above.

Eleven skin cancer images were obtained from different sources [21]. Each image included one or more cancer regions. Some images had heavy hairs and noise. Others had objects such as rules. In these experiments, ground truth data were collected for comparison. Because a single observer's segmentation result is likely to be subjected to observer's bias, it is not suitable to compare the results of computer-aided segmentation with only one observer's manual segmentation results. We, therefore, use the manual outlines of two experienced technicians as ground truth against which the computer-aided delineation is evaluated. Fig. 7 shows the segmentation results. These results show that our algorithm is robust to noise, heavy hair, varying light condition and can extract the boundary of multiple lesion regions. Fig. 8 shows the experimental results measured against Pratt's quality measurement metric. In Fig. 8, the manual delineation from two other experienced technicians which was not used for ground truth was used to compare with that obtained by the computer. Experimental results show that the results obtained by the computer are similar to those obtained by the technicians. The delineation obtained by the computer is closer to the ground truth than that obtained by the second experienced technicians while it is farther than that obtained by the first experienced technicians. The average *FOM* values of the 11 images are 0.702, 0.830 and 0.685 for the delineation obtained by the computer, the first technician and the second technician respectively.

5. Conclusion

We presented a new cancer image segmentation algorithm. The algorithm is composed primarily of two parts. The first part uses an anisotropic diffusion (AD) filter to remove the noise and hairs. The second part uses a multi-directional GVF snake to segment the cancer region in the image. We compared our algorithm with manual segmentation. The experiments show that the performance of the proposed algorithm is close to that obtained by human segmentation.

References

[1] A. Round, A. Duller, P. Fish, Color segmentation for lesion classification, in: Proceedings of the 19th Annual International Conference of the IEEE Engineering in Medicine and Biology society, Chicago, IL, USA, 30 October–2 November 1997, pp. 582–585.

[2] Z. Zhang, W. Stoecker, R. Moss, Border detection on digitized skin tumor images, IEEE Trans. Med. Imaging 19 (11) (2000) 1128–1143.

[3] G. Hance, S. Umbaugh, R. Moss, W. Stoecker, Unsupervised color image segmentation: with application to skin tumor borders, IEEE Eng. Med. Biol. Mag. 15 (1) (1996) 104–111.
[4] F. Ercal, M. Moganti, W.V. Stoecker, R.H. Moss, Detection of skin tumor boundaries in color images, IEEE Trans. Med. Imaging 12 (3) (1993) 624–626.
[5] L. Xu, M. Jackowski, A. Goshtasby, C. Yu, et al., Segmentation of skin cancer images, Image Vision Comput. 17 (1) (1999) 65–74.
[6] D.H. Chung, G. Sapiro, Segmenting skin lesions with partial-differential-equation-based image processing algorithm, IEEE Trans. Med. Imaging 19 (7) (2000) 763–767.
[7] H. Ganster, A. Pinz, R. Rohrer, E. Wilding, M. Binder, H. Kittler, Automated melanoma recognition, IEEE Trans. Med. Imaging 20 (3) (2001) 233–239.
[8] M. Kass, A. Witkin, D. Terzopolous, Snakes: active contour models, Int. J. Comput. Vision 1 (4) (1987) 321–331.
[9] C. Xu, J.L. Prince, Snakes, shapes, and gradient vector flow, IEEE Trans. Image Process. 7 (3) (1998) 359–369.
[10] C. Xu, J.L. Prince, Generalized gradient vector flow external force for active contours, Signal Process. 71 (2) (1998) 131–139.
[11] J. Tang, S. Millington, S. Acton, J. Crandall, S. Hurwitz, Surface extraction and thickness measurement of the articular cartilage from MR images using directional gradient vector flow snake, IEEE Trans. Biomed. Eng. 52 (5) (2006) 896–907.
[12] J. Tang, S. Acton, Vessel boundary tracking for intravital microscopy via multi-scale gradient vector flow snakes, IEEE Trans. Biomed. Eng. 51 (2) (2004) 316–324.
[13] G. Gerig, O. Kubler, R. Kikini, F.A. Jolez, Nonlinear anisotropic filtering of MRI data, IEEE Trans. Med. Imaging 11 (2) (1992) 221–232.
[14] Y. Yu, S. Acton, Speckle reducing anisotropic diffusion, IEEE Trans. Image Process. 11 (11) (2002) 1260–1270.
[15] Q. Sun, J.A. Hossack, J. Tang, S. Acton, Speckle reducing anisotropic diffusion for 3D ultrasound images, Comput. Med. Imaging Graphics 28 (8) (2004) 461–470.
[16] J. Tang, Q. Sun, Y. Cao, J. Liu, An adaptive anisotropic diffusion filter for noise reduction in MR images, in: Proceeding of IEEE International Conference on Mechatronics and Automation, Harbin, China, August 5–8 2007, pp. 1299–1304.
[17] F. Zhang, Y. Yoo, L. Koh, Y. Kim, Nonlinear diffusion in Laplacian pyramid domain for ultrasonic speckle reduction, IEEE Trans. Med. Imaging 26 (2) (2007) 200–211.
[18] M. Black, G. Sapiro, Edges as outliers: anisotropic smoothing using local image statistics, in: Nielsen et al. (Eds.), in: Scale-Space'99, Lecture Notes in Computer Science, vol. 1682, Springer, Berlin,1999, pp. 259–270.
[19] F. Yan, H. Zhang, C.R. Kube, A multistage adaptive thresholding method, Pattern Recognition Lett. 26 (8) (2005) 1183–1191.
[20] W.K. Pratt, Digital Image Processing, Wiley, New York, 1978.
[21] ⟨http://www.meddean.luc.edu/lumen/MedEd/medicine/dermatology/Melton/content1.htm⟩.

About the Author—JINSHAN TANG received the Ph.D. degree from Beijing University of Posts and Telecommunications in 1998. Upon graduation, he joined ATR media integration and communication research laboratories in Japan as an invited researcher. In 2000, he went to Harvard medical school and got one year and half post-doctoral training there. In 2001, Dr. Tang joined the University of Virginia and worked there for about three years. After that, Dr. Tang worked as a visiting fellow in National Cancer Institute, National Institute of Health (Bethesda, Maryland) and senior engineer in Intel in Huston, Massachusetts. Since 2006, he is an assistant professor at Alcorn State University, where he directs the image processing and bio-image research laboratory, which has been supported by DoD funding to develop computer aided breast cancer detection and diagnosis. He teaches in the areas of digital image processing, computer network, and numerical analysis. Dr. Tang's current research interests include image processing and pattern recognition for cancer detection and diagnosis, 3-D human body recognition, MRI and ultrasound imaging. He is an author or co-author of more than 50 papers on image processing. He was a guest editor of Special Issue on Multimedia System Technologies for Educational Tools, (ACM/Springer) Multimedia Systems Journal and associate editor of Proceeding of The 2001 International conference on Artificial Intelligence, Las Vegas, Nevada, USA, June 25–28, 2001, CSREA Press, USA. Dr. Tang served as a session chair of image processing and analysis for oncology in ICIP2007. Dr. Tang is a senior member of IEEE.